Measurement of Velocity in High-Temperature Liquid Metals

A.C. MIKROVAS and S.A. ARGYROPOULOS

There is a paucity of methods available for the measurement of velocity in high-temperature liquid metals. This is due to the hostile environmental conditions which characterize liquid metals. This article proposes and appraises a new velocity measurement technique for liquid metal flows at high temperatures. The melting rates of metallic spheres in metal baths of the same chemical composition as the spheres are studied under isothermal conditions. It is demonstrated that the metallic sphere can be used as a probe for measuring the average velocity in a metal flow system over a distance equivalent to the diameter of the sphere. The system that was chosen for study is the commercial purity aluminum bath. The experimental calibration setup examined three different elements: (a) it introduced a stationary sphere in a metallic bath of a given temperature and compared its melting rate with that of a moving sphere with known external velocity along the periphery of a circle in a metallic bath of the same temperature; (b) three different sphere diameters were used; and (c) a range of bath temperatures was investigated. By studying the effect of these three elements concurrently, it was possible to determine the interplay of these elements. Results showed that the sphere melting time was related linearly to the flow velocity for the range of velocities of 0 to 40 cm/s and for bath superheat up to 100 °C. In order to verify the accuracy of the results obtained by the proposed technique, a comparison was undertaken between mathematical predictions and experimental results of a fluid flow field obtained in an AC induction furnace with molten aluminum. These predictions were made by solving numerically the relevant differential equations under the appropriate boundary conditions. The experimental results attained using the proposed technique were in close agreement with those from the mathematical predictions.

I. VELOCITY MEASUREMENT METHODS IN LIQUID METALS AND THEIR LIMITATIONS

KNOWLEDGE of flow velocities in liquid metal systems is important in the design and control of high-temperature processes from laboratory up to actual industrial scale setups. Some examples of processes where metal flows occur include aluminum reduction cells and continuous casting equipment from the aluminum industry, while from the steel industry, representative examples are flows in tundishes, stirred ladles, induction furnaces, and continuous casting processes.

Velocities averaged over a small region are measured in common fluids based on several different physical principles. They include the following: (a) flow visualization by direct injection-photographic methods, (b) measurement of velocities with differential pressure, (c) electromagnetic velocity measurement, (d) hot wire and hot film anemometry, and (d) Laser-Doppler velocimetry. For the case of liquid metals, opacity rules out flow visualization techniques and photographic methods, except for measurements at free surfaces.[1,2,3] Laser-Doppler velocimetry is also excluded for the same reason. The pitot tube suffers from the difficulty of coupling it to the pressure sensor without freezing liquid in the lines or overheating the sensor. Hot wire and hot film anemometers are also unable to withstand temperatures in excess of approximately 100 °C, so the application of these sensors has been restricted mostly to mercury[4–13] and Wood's metal flows.[14]

In addition to photographic methods and hot wire-film anemometry, the following probe-velocity measurement techniques have been applied in liquid metals: (a) reaction probes, (b) tracer techniques, (c) electromagnetic probes, (d) velocity measurements from dissolution studies, and (e) fiber optic velocity sensor.

The principle of operation of the reaction probe is based on measuring the force exerted on a submerged body by the flowing fluid. Reaction probes have been used in a variety of configurations, depending on the type of submerged body and its positioning: they include horizontal[15] or vertical[16,17] discs or plates and porous spheres.[18–22] The most sophisticated probe of this type is the one by Moros *et al.*,[22] since it can simultaneously measure two-dimensional velocities. However, this probe has been used only in low-temperature studies (mercury pools). The other reaction probes have the following limitations: (a) they measure only one velocity component,[15,16,17] (b) they have been used only in low-temperature studies,[15,18–20,22] (c) they have been used to measure velocities only close to free surfaces,[17,21] and (d) for the case of the sphere, the Reynolds number must be in the range of 2×10^3 to 2×10^5 in order for the drag coefficient to be insensitive to the Reynolds number.[23]

The tracer method has been applied for velocity and diffusivity measurements in molten metals over the years. In this technique, a small amount of tracer is introduced at some point in the flow field while the melt may be periodically sampled at downstream locations. Typically, the concentration of the tracer at a downstream location can be expressed as a function of distance (from the tracer injection point), the time of the

A.C. MIKROVAS, formerly Graduate Student, Department of Metallurgy and Materials Science, University of Toronto, is Research Engineer, Cominco Ltd., Trail, BC, Canada. S.A. ARGYROPOULOS, Associate Professor, is with the Department of Metallurgy and Materials Science, University of Toronto, Toronto, ON, Canada M5S 1A4. e-mail address: argyro@ecf.utoronto.coc.

Manuscript submitted July 16, 1992.

sampling, the diffusivity, and the average flow velocity. By fitting the measured concentration curve to the mathematical formulation of the previous function, the velocity and diffusivity can be found. Velocity and diffusivity measurements have been reported by Grjotheim and co-workers[24,25,26] in studies of aluminum reduction cells. Szekely[27] used a radioactive tracer to measure the turbulent diffusivity within the metal in an open-health furnace. Nakanishi *et al.*[28] reported on tracer dispersion and deoxidation studies in an ASEA-SKF furnace, and subsequently, Szekely and Nakanishi[29] calculated flow and tracer dispersion from first principles. Measurement of velocities in both industrial and laboratory scale units using radioactive tracers has been reported by Szekely and Chang.[30] The melts were aluminum or steel, and the experimental velocities were compared to those computed using theoretical principles, the modeling work being described in References 30 and 31. In all cases, measurements and theoretical predictions agreed within a factor of 2. Tracer techniques are, in general, useful for predicting the order of the mixing characteristics of a system. However, with respect to flow velocities, they suffer from interpretation problems because of mismatches between particle and fluid velocity, especially under turbulent flow conditions.[32] Another disadvantage is that the calculated flow velocities are average values over a large distance.

The application of electromagnetic principles for velocity measurements in duct flows has been extensively used in the industry over the years. However, it was just in the last decade that such a principle was applied for local velocity measurements. The original measurement method is described in Reference 33 and was subsequently perfected[34] and used in various studies.[35–38] The innovation by Vives and co-workers[33,34] replaced the magnetic field of external origin with the one produced by a small cylindrical permanent magnet which was incorporated in the probe. It is essentially made up of a cylindrical permanent magnet and two pairs of antipodal electrodes situated at the midheight of the magnet. A voltage is produced between the electrodes depending on the local temperature and flow velocity, the relationship between velocity and voltage at constant temperature being linear. The probe can measure velocities in liquid metals at temperatures up to approximately 720 °C. Other than the temperature limitation, the probe has the disadvantage that its lifetime in liquid aluminum melts is rather limited.[39,40]

The measurement of metal velocities from the mass loss of iron rods introduced in liquid aluminum was initially developed by Johnson.[41] Johnson, and subsequently Tabereaux and Hester,[42] derived calibration curves correlating mass loss with metal velocity by measuring the iron rod mass loss in a stirred tank. The discrepancies that were present in early calibrations were subsequently rationalized by Bradley *et al.*[43] and were attributed quantitatively to differences in metal temperature. Last, a very interesting study by Pant *et al.*[44] showed that the results from dissolution of stirred rods in stationary liquid and suspended rods in a flowing stream are in very good agreement. A rather similar technique has been used for fluid flow measurements in a steel melt by El-Kaddah *et al.*[16] Melt velocities were measured experimentally from the study of the rate at which carbon rods dissolve in low carbon steel melt. By determining the extent of dissolution for specific time intervals, the local mass transfer coefficients were calculated and were compared to those predicted using both laminar[45] and turbulent[46] correlations:

$$\mathrm{Sh} = 0.683\ \mathrm{Re}^{0.466}\ \mathrm{Sc}^{1/3} \quad [1]$$

$$\mathrm{Sh} = 0.338\ (\mathrm{Re}\ \mathrm{Tu})^{0.8}\ \mathrm{Sc}^{1/3} \quad [2]$$

The values for the Reynolds number, Re, and the turbulent intensity, Tu, were input to the previous relationships from the results of a numerical model of the 4-ton induction furnace, where the experiments were carried out. From the results reported in that study,[16] the laminar flow correlations tended to underpredict the mass transfer coefficient by an order of magnitude, and when using the turbulent correlations, the mass transfer coefficient was within a factor or two of the measurements. It should be noted that correlation[2] was produced from the study of melting rates of ice rods in water under recirculating flow conditions;[46] the average local and fluctuating components of the water velocity were measured in a previous study by Grevet *et al.*[47] using laser anemometry.

A fiber-optic velocity sensor has been developed for velocity measurements in liquid metal flows.[48] The sensing element is formed as a thin-walled glass cone with a glass pointer sealed in its end. The free end of the pointer is blackened and placed in the air gap between the two pairs of light guides, two of which are optically connected to the source of light and the other two to the photocells. The light guides form two perpendicular beams of light in the air gap. In its initial position (zero velocity), the pointer intercepts partially the two beams. Under the flow action, the sensing element deflects and the pointer changes the amount of light reaching the photocells by changing its position. Thus, the values of the electric signals from the photocells depend on the values of the two velocity components. The fiber-optic sensor has been used for velocity measurements in mercury flows,[48] while it is known to have been used in studies in liquid aluminum.[49]

In summary, the review on existing velocity measurement methods shows that of the few studies conducted in liquid metals at high temperatures, there is no consensus as to the most appropriate method.

II. AIMS OF THE STUDY

There are three aims in this study. First, to propose a new velocity measurement method which can be applied to liquid metals especially at temperatures beyond 700 °C. Second, to use this method to measure the fluid flow velocity in an AC induction furnace containing liquid aluminum. Third, to assess the validity of this method by comparing experimental results derived by using this method with mathematical predictions of fluid flow in an AC induction furnace.

The method introduces metallic spheres of identical chemical composition with the melt where velocity measurements are to be performed. The melting time of the metallic sphere in the liquid metal and at the specific

immersion point is experimentally measured and is directly related to the metal velocity. This is achieved by performing proper calibration experiments in the same liquid metal system, where the melting time of the sphere is correlated to the metal velocity, which is imposed and controlled externally. The temperature fields in both the actual measurement system and the calibration system should be identical.

III. METHODOLOGY

A. *Bath-Probe System Part (A)*

The system that was evaluated as the most suitable for testing the applicability of the proposed velocity measurement method was the commercial purity aluminum bath. Metallic spheres of identical chemical composition with the bath were selected for the construction of the probe. The bath temperature was desired to be slightly above 700 °C for the initial sets of tests, since this is the approximate temperature limit for the electromagnetic probe.[34] At these temperatures, the aluminum bath superheat is relatively low, which makes the probe more sensitive to the flow velocity as compared to higher superheats. In contrast, the rather high thermal conductivity of the metallic melt provides a good test for the sensitivity of the probe with respect to flow velocity. The reasons for choosing the sphere's material to be the same as that of the bath are as follows.

(a) Mass transfer between sphere and metal bath may take place only by melting mechanism.
(b) For all cases in which the sphere and melt material are not identical, the melting process contaminates the bath. This is highly undesirable for most laboratory and plant experiments.

A schematic diagram of the probe that was used is shown in Figure 1. It should be noted that three sizes of spheres were used, 2.5, 3.0, and 3.5 cm in diameter. The probe configuration was the same for all three sizes, with the exception of the sphere itself and the lower stainless steel part which had a larger external diameter for the 3.5-cm-diameter sphere. The upper part of the probe consists of a nonmagnetic stainless steel holder; in its lower end is inserted a zirconia tube which, in turn, is inserted into a threaded stainless steel part that screws to the sphere. The drilled portion of the sphere represents approximately 7 pct of its volume, while only the upper part of the cylindrical cavity is threaded so that the stainless steel part fits in. The reasons for the selection of the zirconia tube as a link between the holder and the lower stainless steel part are primarily its low thermal conductivity (in the order of 2.5 W/m/K for the temperatures in the present study) and its rather reasonable resistance to thermal shock. The selection of the high-temperature alumina cement (989 from Cotronics Corp.) was based primarily on its low thermal conductivity, while the coupling of the three parts—lower stainless steel part, zirconia tube, and stainless steel holder—was rigid for four to five experimental runs. Both the zirconia tube and the alumina cement because of their low thermal conductivity, allowed for rather small heat losses from the aluminum sphere to the holder.

It should be made clear that the errors introduced because of the deviation from the ideal case, where the sphere is suspended without support in the bath, are important only in calculating the actual energy input to the sphere. It is only in this case that every error should be quantified and kept as low as possible, since the use of results in this generalized form does not refer to a specific holder-sphere configuration. Otherwise, correlating data in the simple form of melting time *vs* flow velocity (for a specific probe construction) is rather an easy task. In this case, it is critical that the actual experiments are carried out under similar conditions as the calibration procedures, *i.e.*, any heat losses, are the same in both cases.

The principle of the probe is based on measuring the time it takes for the sphere to melt upon immersion in the liquid metal. The exact time that the sphere is immersed in the bath is recorded in two different ways, depending on the experimental setup. In one arrangement, for example, part B of the study, an external thermocouple was used which recorded the time the sphere was immersed in the liquid metal. For part C of the study, the immersion time was recorded by means of a load cell, from which the proposed probe was suspended throughout the test. Finally, for all components of the study, the total melting time of the sphere was monitored by means of the internal thermocouple, which is intentionally positioned within the cylindrical cavity without touching the walls of the cavity. This is shown in the schematic diagram of the assembled probe presented in Figure 1.

B. *Calibration Technique (Part B)*

Figure 2 provides a general view of the apparatus for stirring spheres in liquid aluminum held in a crucible in an induction furnace. It consists of an outside frame, a carriage that slides along the vertical steel poles of the frame, and the pulleys-counter weights arrangement that enables the vertical motion of the carriage. Detail of the carriage is shown in Figure 3. A DC motor is mounted on the carriage and is denoted by the letter (A). The motor rotates a big sprocket, denoted by (B), which, in turn, through a chain (C) transmits the motion to a system of sprockets (D) rigidly attached to the upper end of a vertical hollow shaft (E). The support of the vertical shaft consists of an aluminum block (F) rigidly mounted on the carriage and machined so that the shaft passes through; at the periphery of the machined bore, a bearing is placed that allows for the shaft to rotate. The bottom of the shaft is screwed to an aluminum disc (G). At a selected radial position on the disc, the upper end of the proposed probe holder (H) is rigidly screwed. At the upper opening of the vertical hollow shaft is placed a rotor receptacle of a slip ring assembly. The insulated wires at the bottom of the receptacle are connected to the probe thermocouple using extension wires (I) that run through the hollow shaft. The upper end of the rotor receptacle is connected to an insulated stator (J), which, in turn is connected through extension wires to a K-type module of the data acquisition system. The number of rotations of the large sprocket is continuously monitored as a function of time using an absolute encoder which

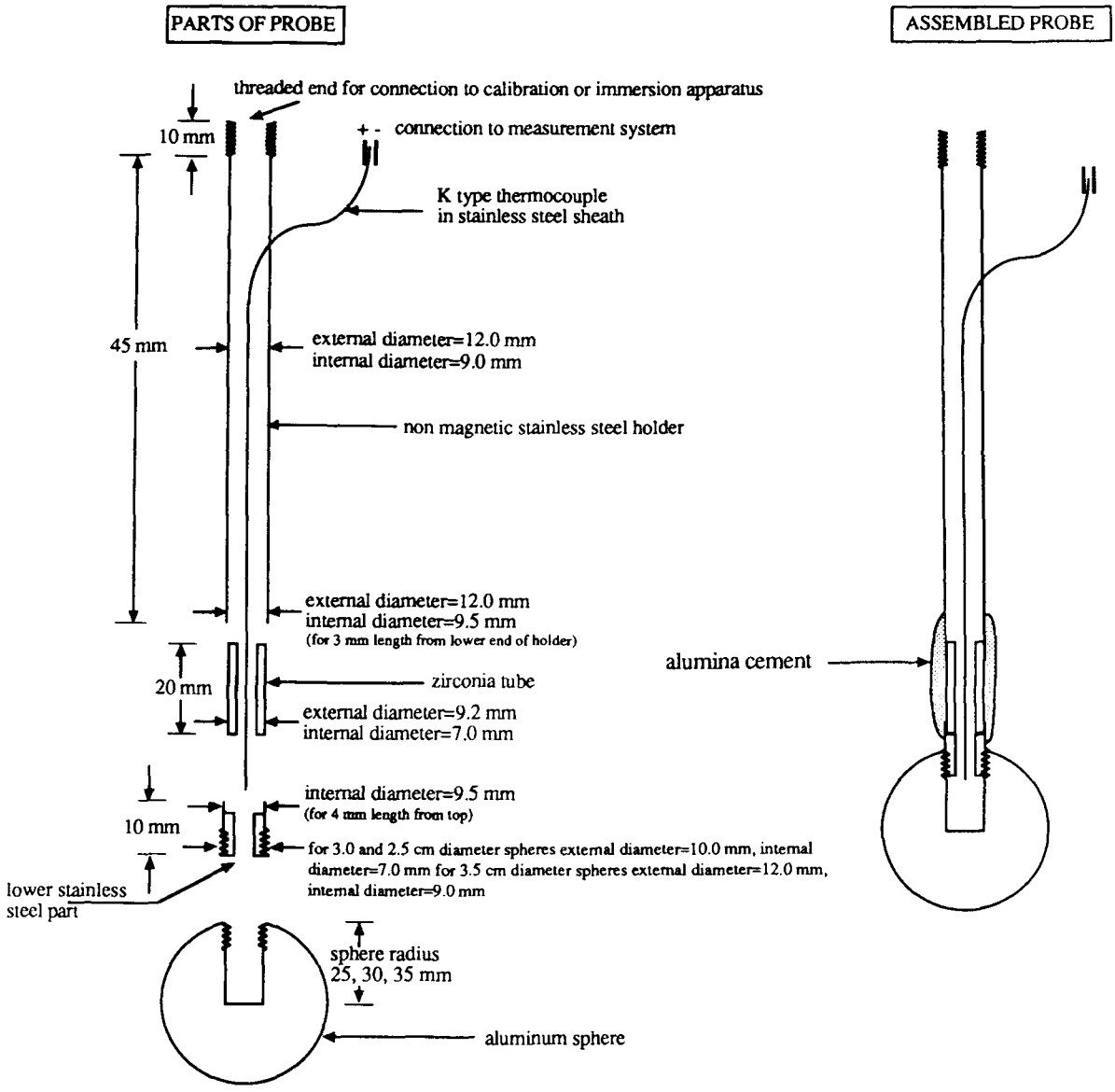

Fig. 1 — Schematic diagram of the probe used in the liquid aluminum.

is connected to the data acquisition system. Finally, the angular velocity of the big sprocket is adjusted from the motor control unit. The exact time that the sphere is immersed in the liquid metal is recorded by means of an external thermocouple that hits the surface of the hot water simultaneously with the immersion of the sphere in the liquid metal.

The execution of a typical experiment includes the following: (1) bringing the metallic bath to a specific temperature (preliminary experiments for mapping the temperature field in the melt showed that it was approximately isothermal); (2) adjustment of the angular velocity of the disc; (3) turning off the induction furnace so that there is no flow in the bath because of the electromagnetic body forces (the maximum time that the furnace was off for this type of experiment was approximately 30 seconds); (4) immersion of the probe at a desired depth in the liquid metal; and (5) collection of the data from the sensors (two bath thermocouples located at the same depth as the probe and within 2 cm of radial distance from the probe, the external thermocouple, the probe thermocouple, and the absolute encoder). Figure 4 shows a schematic diagram of the data acquisition system.

C. *Results (Part B)*

Figure 5 shows a typical experimental result. Two representative bath temperature readings are shown by curves 1 and 2, which clearly demonstrate that the difference between them is in the range of the accuracy of the K-type thermocouples that were used. Curve 4 is the temperature profile of an external thermocouple. It is initially suspended in air, segment AB, and it hits the surface of hot water, segment BC, simultaneously with the immersion of the probe in the liquid metal. Finally, it stays at a constant temperature, segment CD, for the period the probe is inside the melt. Curve 3 is the temperature profile recorded by the probe thermocouple positioned as shown in Figure 1. Segment EF records

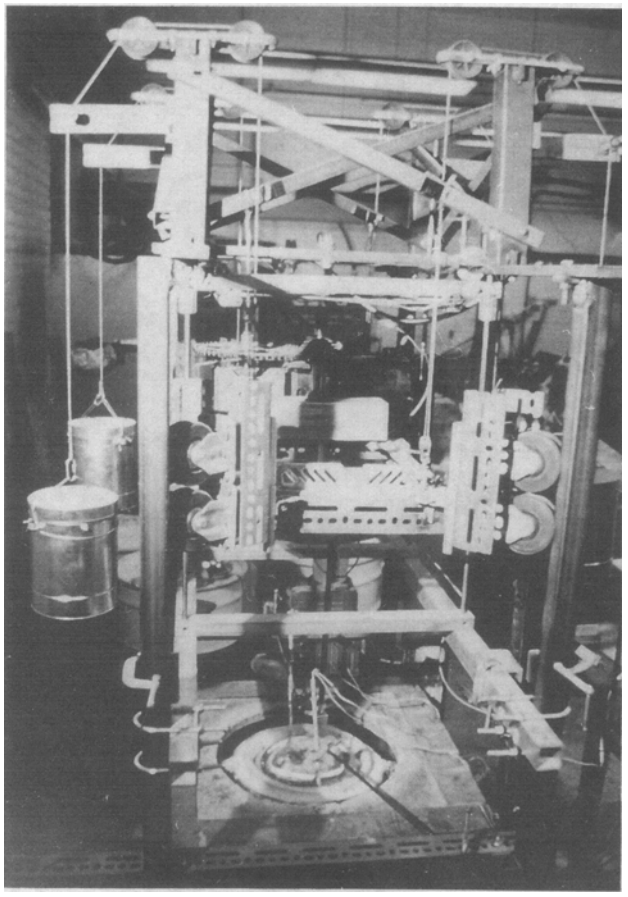

Fig. 2—The experimental setup for stirring spheres in liquid aluminum.

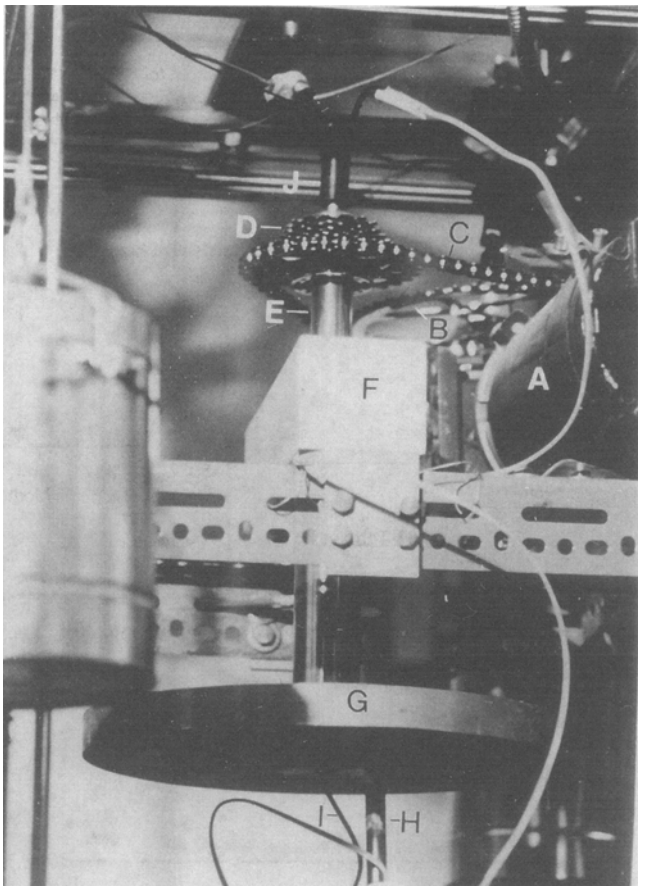

Fig. 3—Detail picture of carriage construction for stirring spheres in liquid metal. (A) motor, (B) big sprocket, (C) chain, (D) gears, (E) hollow shaft, (F) aluminum block, (G) disc, (H) probe holder, (I) wires connecting rotor receptacle, and probe thermocouple, and (J) insulated stator.

the temperature at the thermocouple tip location in the sphere cavity before the probe is immersed in the bath. Point F is taken as the immersion point (projection of point B on curve[3]). Segment FG corresponds to the lag of the probe thermocouple to record immersion of the sphere in a high-temperature environment. This is because the thermocouple tip is intentionally stationed in the air, inside the drilled cavity of the sphere. Segment FGH characterizes the heating period of the sphere. At point H, the slope of the curve changes dramatically, indicating that liquid metal penetrates into the sphere cavity. In an extremely short time interval, the thermocouple records the melting temperature of aluminum (660.2 °C, curve (5)) at point I, the intersection point of curves 5 and 3. Segment IJ corresponds to the heating of the thermocouple tip above the aluminum melting point.

It should be mentioned that the probe thermocouple should finally record the local bath temperature, denoted by segment JK. The actual local bath temperature is presented by curve 6 and is recorded by an independent K-type thermocouple at the end of the experiment. The reason for the difference (20 °C to 30 °C) between the reading of the probe thermocouple and the one shown by curve 6 was attributed to the slip ring assembly and the cold junction compensation system through which the probe thermocouple signal was transmitted to the data acquisition system.

From the above analysis, it can be seen that the time it takes for the sphere to melt can be determined by the projection of points B and I on the time axis, that is, segment RS. It should also be mentioned that in characterizing the whole experiment there is also the need for recording the temperature at the surface of the sphere before immersion. Such measurements were taken prior to each experiment using K-type thermocouples. The average surface temperature of the sphere was in the range of 40 °C to 50 °C for the bulk of the experimental work reported in this study.

At this point, results will be presented for all three sphere sizes for a range of tangential velocities at the center of the sphere between 0 and 45 cm/s and for a bath superheat of 40 °C to 100 °C. In all of these experiments, the sphere was immersed at a depth of 7.0 cm below the bath surface, the rotation occurred on a circle with diameter 13 cm, and the distance between the center of the sphere and the crucible wall was 9.5 cm. The results will be presented in the form of plots where the sphere velocity (y-axis) is plotted against the measured melting time (x-axis). At the top right corner of each graph will be shown the regression formula for the plotted data together with the respective correlation coefficient.

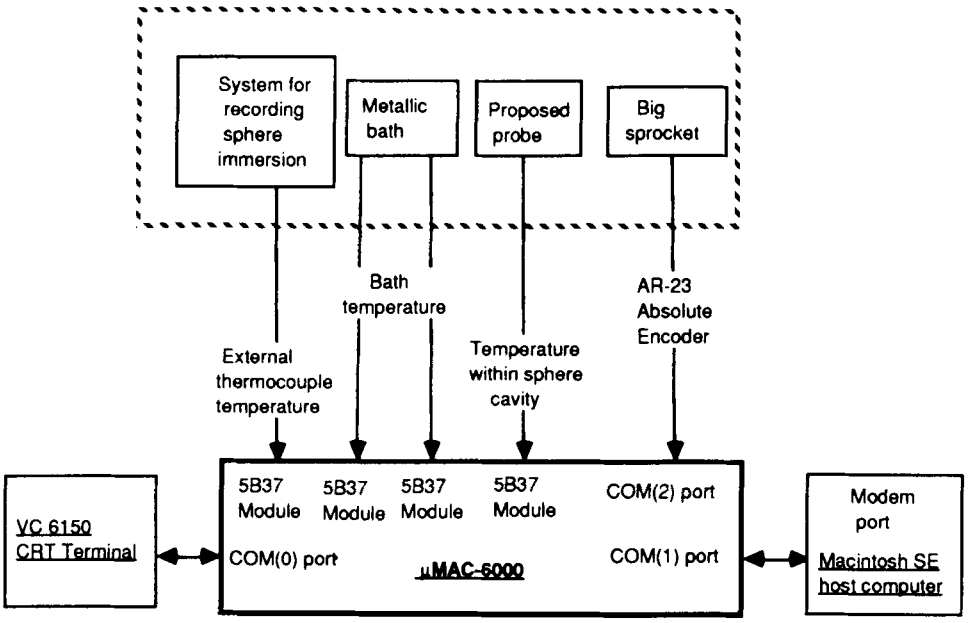

Fig. 4—Schematic diagram of the data acquisition system.

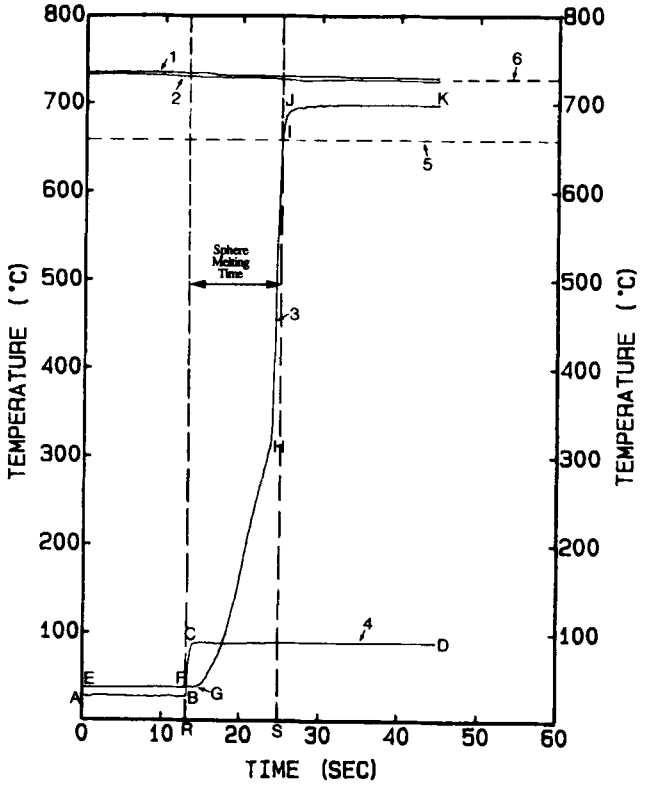

Fig. 5—Typical experimental results using the probe with one external thermocouple. Curves 1 and 2: representative bath temperature readings at different locations in the aluminum bath. Curve 3: temperature profile of probe thermocouple. Curve 4: temperature profile of external thermocouple that records immersion time. Curve 5: aluminum melting point. Curve 6: temperature reading of independent thermocouple at the sphere immersion point at the end of the experiment.

1. *3.5-cm-diameter spheres*

A number of experiments were conducted with 3.5-cm-diameter aluminum spheres. Figure 6 presents three sets of tests representing the three aluminum bath temperatures studied. Studying these results, the following comments can be made.

(1) A first order polynomial provides a satisfactory correlation.
(2) The higher the velocity of the sphere, the lower its melting time for each specific bath temperature range.

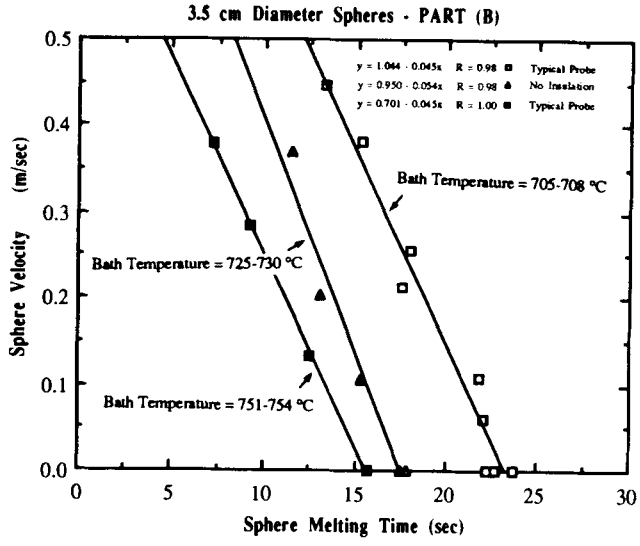

Fig. 6—Sphere velocity *vs* melting time for the 3.5-cm-diameter spheres for all bath temperature ranges studied (part B).

(3) From a comparison of all three sets of results, presented in Figure 6, and for the same sphere velocity, the higher the bath superheat, the lower the melting time of the sphere.
(4) The results obtained for the bath temperatures of 705 °C to 708 °C and 751 °C to 754 °C used the typical sphere holder (thermally insulated end) and therefore, have identical slopes. In the case of the plain steel holder (bath temperature 725 °C to 730 °C), on the other hand, the slope is higher. This can be justified by the fact that heat losses from the sphere to the holder are larger in the case of the plain holder, reflecting on a longer sphere melting time (with reference to melting time at zero external velocity for each set).
(5) From the results where the typical holder design was used and for the range of velocities that were studied, the maximum difference in the recorded melting times is approximately 10 seconds.

2. *3-cm-diameter spheres*

A number of experiments were conducted with 3.0-cm-diameter aluminum spheres and for the bath temperature range of 705 °C to 710 °C. Figure 7 presents the results obtained. The slope of the curve is almost the same as the one recorded from the 3.5-cm-diameter sphere experiments and for the temperature range 705 °C to 708 °C. A comparison between these two sets of results (Figure 7) indicates that for the case of 3.0-cm-diameter spheres, the curve is shifted to the left, thus showing faster melting of those spheres as compared to the 3.5-cm-diameter spheres for the same velocities.

3. *2.5-cm-diameter spheres*

A number of experiments were conducted with 2.5-cm-diameter aluminum spheres and for the bath temperature ranges of 700 °C to 705 °C and 752 °C to 756 °C. Figure 8 presents the results obtained. The curves present similar trends to the ones reported earlier for the 3.5-cm-diameter spheres. The slope of the curve for the low-temperature data is in the same range as the low-temperature data for both 3.5- and 3.0-cm-diameter spheres. The only exceptions are that the slope for the high bath temperature data is higher and the correlation coefficient is lower. The reason for the increase of the slope of the curve for the case of high bath superheat may be attributed to the fact that the effect of bath superheat is more dominant over the effect of flow velocity. The mass of the sphere is much smaller, approximately 18 g, as compared to 36 and 58 g, respectively, for the 3.0-cm and 3.5-cm-diameter spheres. In this case, the energy requirements for melting the sphere are smaller, which makes the method less sensitive to flow velocity. Since the sphere melting time range at this superheat and sphere size is smaller as compared to the lower temperature data, it is more suitable that larger size spheres be used for velocity measurements at these bath temperatures.

Finally, Figure 9 presents the experimental results for all three sizes of spheres for the low bath temperature range, while Figure 10 presents a summary of the results for all sphere sizes and bath temperature ranges for part

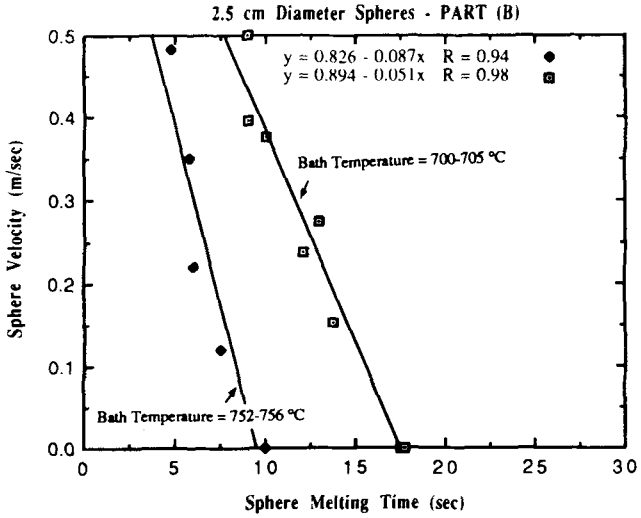

Fig. 8—Sphere velocity *vs* melting time for the 2.5-diameter spheres for bath temperature ranges 700 °C to 705 °C and 752 °C to 756 °C (part B).

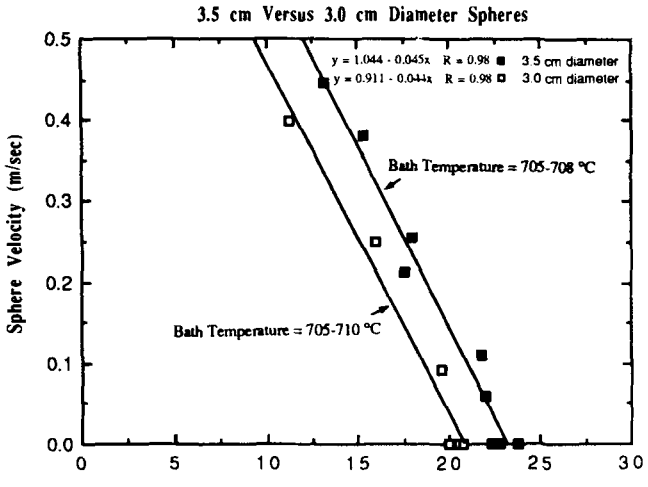

Fig. 7—Sphere velocity *vs* melting time for the 3.5-cm and 3.0-diameter spheres for bath temperature ranges 705 °C to 708 °C and 705 to 710 °C, respectively.

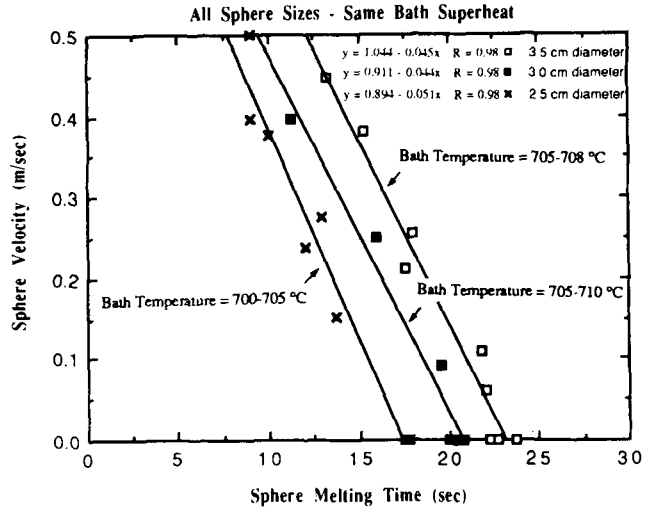

Fig. 9—Sphere velocity *vs* melting time for the three sizes of spheres studied and for the lowest bath temperature range (part B).

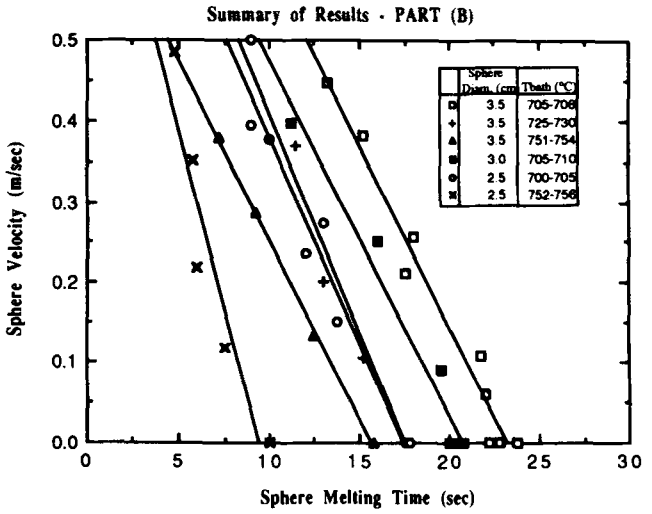

Fig. 10—Compilation of all data obtained in part B.

B of the study. Figure 10 shows the effect of sphere size, bath superheat, and sphere velocity on the sphere melting time in a single graph.

IV. REPRODUCIBILITY AND ACCURACY

A number of experimental results are presented in Table I assessing the reproducibility of each set of tests.

Table I. Results from Experiments on Reproducibility (Part B)

Velocity (m/s)	Melting Time (s)	Mean Melting Time (s)	95 pct Confidence Interval
0.035-m-Diameter Spheres, 705 °C to 708 °C			
0.0	23.75		
0.0	22.75	22.92	±2.32
0.0	22.25		
0.035-m-Diameter Spheres, 725 °C to 730 °C			
0.0	17.50		
0.0	17.90	17.70	±3.59
0.030-m-Diameter Spheres, 705 °C to 710 °C			
0.0	20.75		
0.0	20.50	20.42	±1.16
0.0	20.00		
0.030-m-Diameter Spheres, 747 °C to 749 °C			
0.1154	11.00		
0.1132	10.25	10.58	±1.16
0.1139	10.50		
0.030-m-Diameter Spheres, 723 °C to 724 °C			
0.3448	10.75		
0.3466	10.25	10.25	±1.52
0.3498	9.75		
0.025-m-Diameter Spheres, 752 °C to 756 °C			
0.0	17.75		
0.0	17.50	17.58	±0.44
0.0	17.50		

Column 4 in Table I presents the reproducibility calculated for a typical 95 pct confidence interval. The reproducibility of the results is influenced by (1) temperature control in the bath, (2) speed of immersion of the probe, (3) surface temperature of the sphere before immersion, and (4) consistency in making each probe. In establishing a calibration curve, it is desirable that the temperature of the bath is the same for each individual experiment. In this study, the temperature was controlled manually, as was the speed of immersion of the probe. In general, it is preferable that the immersion time be as small as possible and be the same for all the calibration experiments. In controlling the initial temperature of the sphere, it is desirable that the initial position of the probe is not in close proximity with the furnace. In this research work, the initial surface temperature of the sphere was monitored and kept around 40 °C to 50 °C for most of the experiments.

In discussing the accuracy of the calibration method, the following issues must be addressed. (1) Does the rotation of the sphere with certain tangential velocity give the same result in terms of the sphere melting time as when the sphere is stationary and the fluid moves against it at the same velocity? (2) What is the effect of the sphere size on the measurements? (3) Do the dimensions of the furnace or reactor have an effect on the measurement technique? The first issue has been addressed in dissolution studies.[41,44] Pant *et al.*[44] demonstrated the validity of the calibration technique,[41] where a rod is stirred in a liquid at a certain velocity, by comparing the mass loss data with that obtained in a channel flow where the fluid is flowing past a stationary rod. The correlations between mass loss and flow velocity were linear and identical for the two geometries.

The sphere size may have an effect on the measurements when its radius is large compared to the radius of the rotation or the dimensions of the vessel that holds the metal. In general, it is desirable that both the dimensions of the crucible that holds the liquid metal and the radius of the rotation are large compared to the radius of the sphere. However, as will be shown in part C of the study, when the calibration results from all sphere sizes were used to interpret actual measurements in an unknown flow field, the error was on the order of 10 pct.

The reproducibility of the calibration results can be further improved using equipment that satisfies the four factors mentioned earlier. However, based on results from dissolution studies, where a similar calibration procedure was evaluated, one can claim that the proposed technique simulates to a high degree of accuracy the flow past a stationary sphere.

V. MEASUREMENT OF AVERAGE VELOCITIES IN A LABORATORY INDUCTION FURNACE WITH MOLTEN ALUMINUM (PART C)

The study involved melting rate measurements of spheres in the induction furnace where the calibration

experiments (part B) were conducted earlier. The primary task was to measure the melting time of spheres in liquid aluminum with the power to the furnace on and at exactly the same radius and depth where the calibration experiments of part B of the study were performed. The experiments were conducted at the bath temperature range of 702 °C to 707 °C. This allowed for the conversion of sphere melting time to average velocity at the immersion point using the calibration results (part B) for that bath temperature range. This temperature range was selected, because the authors decided to model both electromagnetic aspects and fluid flow in the induction furnace for this temperature range and compare the modeling results (part D) to the experimental ones (part C). Also, in this part of the article, results are presented that show the effect of the immersion depth of the sphere in the liquid metal on its melting time.

A. *Experimental Setup (Part C)*

The experimental setup was similar to the one used in part B of the study, with the exception that the carriage assembly was modified so that only a load cell was attached to it. The proposed probe was connected to the load cell so that it recorded the apparent weight of the probe. This setup facilitated the positioning of the probe at the desired radial position and depth in the melt. The data acquisition system had the same configuration as described earlier in part B with the exception that the external bath thermocouple was substituted by the load cell.

The liquid aluminum temperature was brought to the desired level and the experiments were conducted with the power to the furnace on. Figure 11 shows a cross section of the induction furnace. The crucible was almost filled with liquid aluminum (line AB). The immersion point where the calibration experiments in part B were conducted is shown as point E.

B. *Results (Part C)*

Figure 12 presents a typical experimental result. Curves 1 through 3 record the same experimental variables as in Figure 5, while curve 6 in Figure 12 depicts a comparable function as curve 4 in Figure 5. Curve 6 shows the output voltage from the load cell as a function of time. Before immersion of the probe in liquid aluminum, the load cell records the weight of the probe in air (segment LM). After point M, vibrations are recorded because the platform of the load cell is moving downward in order for the probe to be immersed in the liquid metal. At point O, the probe is immersed at the desired location in the melt. Part OP corresponds to the heating period of the sphere in the melt and is a rather flat profile. The reason that there is no detectable change in the net downward force during the melting of the sphere is because the densities of solid and liquid aluminum do not differ significantly.

The results from the experiments conducted at the same immersion point as the experiments in part B of the study, point E in Figure 11, are presented in Table II

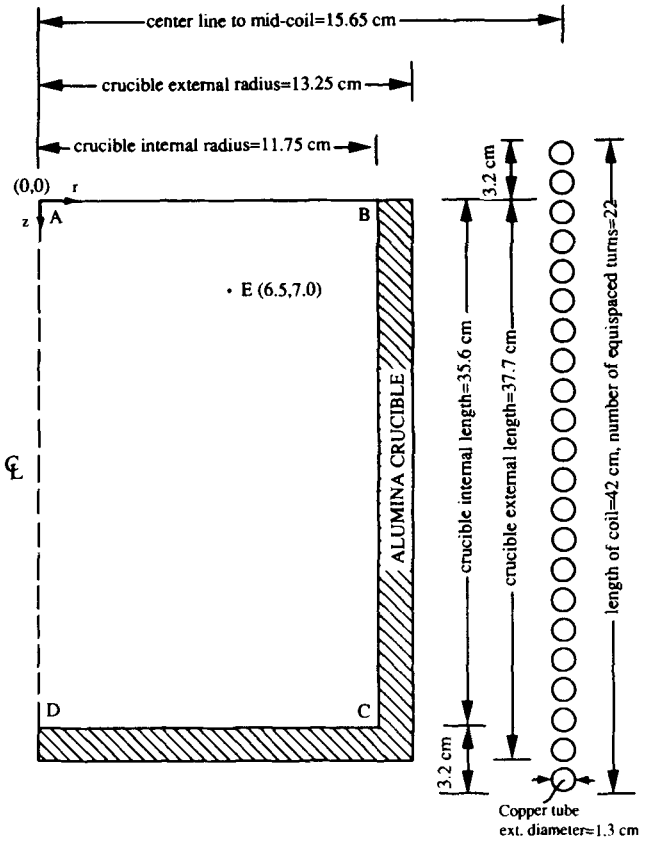

Fig. 11—Schematic cross section of crucible-coil configuration in part B of the study.

($r = z = 0$ at the top surface and center of the melt). With the use of the regression formulas obtained from the calibration tests from part B of the study, the sphere melting times are converted to flow velocities. From this conversion, the rounded velocities are 8 cm/s for the 3.5-cm-diameter spheres, 10 cm/s for the 3.0-cm-diameter spheres, and 9 cm/s for the 2.5-cm-diameter spheres.

An analysis attempted on the melting times of spheres immersed at various other locations in the induction furnace under the same operating conditions showed that for spheres immersed just below the bath surface, the melting time increased by a maximum of 35 pct (compared to the experiments at $z = 7$ cm), while at depths greater than 7 cm, the melting time decreased by a maximum of 12 pct. The radial locations of the center of the sphere for radii between 0 and 6.5 cm were within 10 pct of the results shown in Table II. Trends cannot be identified easily, since the measured melting times depend both on the flow velocity and the distance of the probe from the boundaries of the melt. The preceding results show that the effect of the geometry of the flow system is critical in evaluating the sphere melting time measurements. In order for the flow field to be totally mapped in such a system, there is a need for additional calibration data as a function of distance from the melt boundaries.

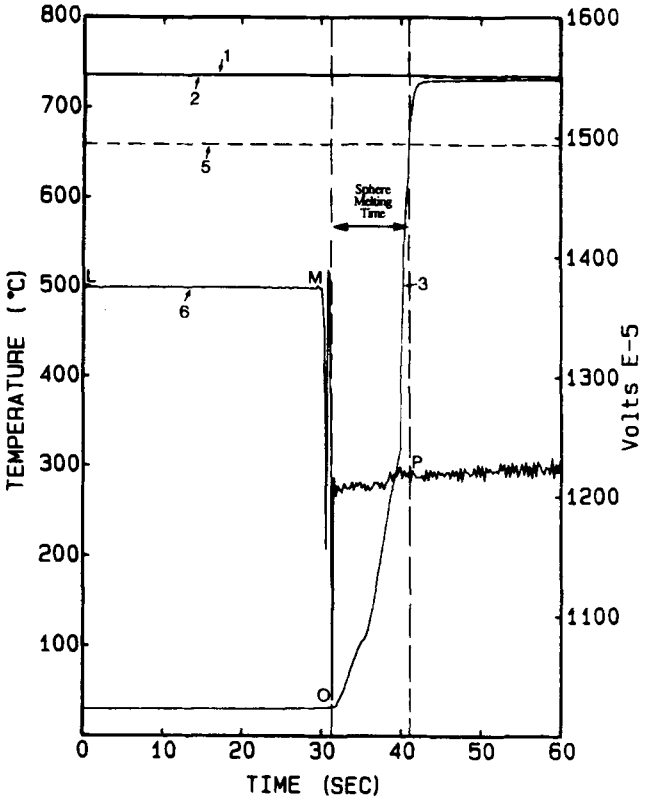

Fig. 12—Typical results using the proposed probe connected to a load cell. Curves 1 and 2: representative bath temperature readings. Curve 3: temperature profile of probe thermocouple. Curve 5: aluminum melting point. Curve 6: output voltage profile from the load cell.

VI. MATHEMATICAL AND NUMERICAL MODELING OF FLUID FLOW IN AN INDUCTION FURNACE (PART D)—COMPARISON WITH THE EXPERIMENTAL RESULTS OF PART C

In an attempt to independently assess the validity of the proposed experimental method, a mathematical model of the fluid flow in an induction furnace with molten aluminum was developed. The electromagnetic forces that were fed to the flow differential equations were calculated by solving the Maxwell equations using the Magnet-2D finite element commercial package. The Navier-Stokes equations for turbulence, coupled to the equations of turbulence according to the low Reynolds number $\kappa - \varepsilon$ model,[50] were solved. The mathematical model for the fluid flow is presented in the Appendix. The numerical method that was used for solving the flow equations is the control volume finite difference method which is described in detail in Reference 51. The model was constructed for exactly the same values of the involved parameters (input current to coil, frequency, crucible-melt configuration) as in the calibration studies (sphere rotation) and for the low-temperature range.

The results are presented in Figures 13 and 14. Figure 13 shows the streamline configuration, while Figure 14 shows the velocity field obtained. These results were gathered with the computational domain divided into a 14 × 21 grid (21 grids in the z direction).

Table II. Sphere Melting Time-Average Velocity at Point E

Average Bath Temperature (°C)	Melting Time (s)	Sphere Diameter (cm)	Average Velocity (cm/s)
703	21.5	3.5	8
707	18.5	3.0	10
704	15.8	2.5	9

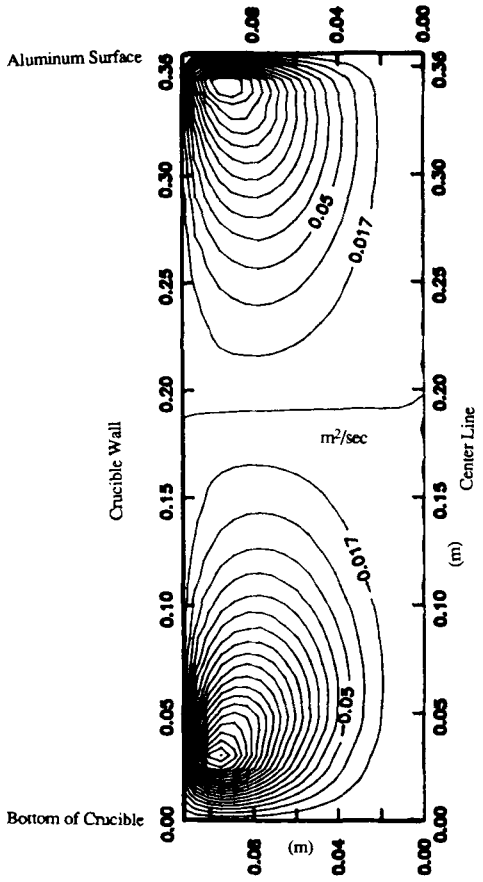

Fig. 13—Streamline configuration from numerical results.

Typically, the computer time requirements were about 50 seconds on a Cray supercomputer. The qualitative nature of the results agrees with the ones theoretically expected. The metal flow in the induction furnace is described as a double torroidal flow.

Based on the experimental results presented in the previous section for the flow velocities in the AC furnace and the numerical ones presented here, it is seen that they agree within approximately 5 cm/s (factor of 2 to 3). The values of the numerically predicted velocities at the sphere immersion point are between 3 and 4 cm/s. This agreement seems to be reasonable if the following factors are taken into account:

(1) An experimental error in the range of 2 to 3 cm/s

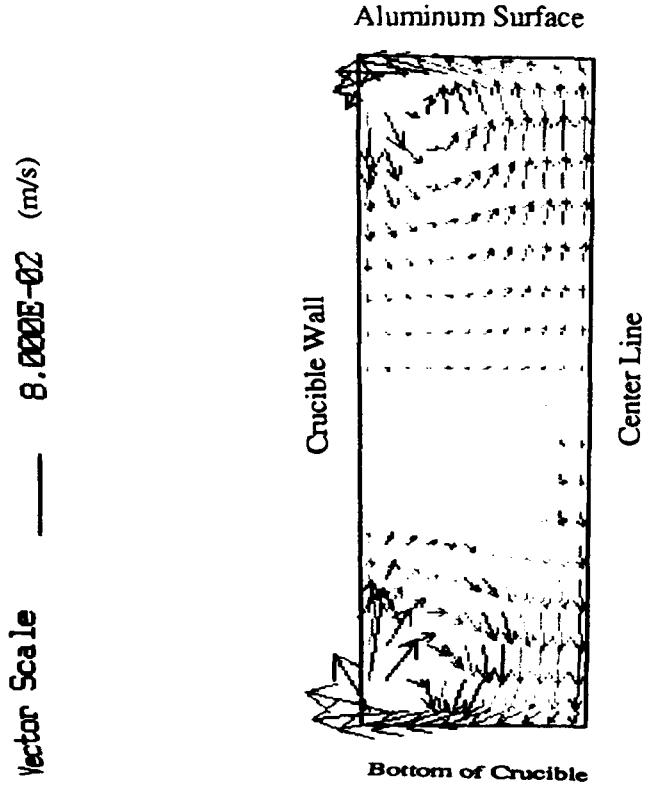

Fig. 14—The velocity field in the induction furnace from the numerical model.

translates to a large percentage error, because the velocities in the induction furnace in the vicinity of the sphere immersion point have low values. Also, it should be kept in mind that zero velocity (externally imposed) for the calibration results does not exclude the existence of very small velocities because of natural convection phenomena.

(2) There are limitations in the degree of accuracy of the numerical results because of the use of the $\kappa - \varepsilon$ model of turbulence. The present formulation of the model of turbulence under the conditions encountered in the induction furnace does not take into account the effect of the existence of external body forces or pressure gradients in the region close to the crucible wall.

(3) The effect of the local turbulence characteristics of the flow field on the melting time of the immersed sphere is not theoretically or experimentally documented. However, as was shown from results from dissolution studies,[46] the intensity of turbulence plays an important role in the mass transfer that takes place between the immersed object and the bath.

(4) The error associated with the assumption of a flat bath surface instead of the meniscus shape possibly contributes to the deviation between numerical and experimental predictions.

From low-temperature studies in mercury, the agreement that has been reported between modeling results and experimental measurements in induction furnaces is almost identical. Similar results have also been reported from the use of the electromagnetic probe in induction furnaces. However, from dissolution studies, agreement between experimental and numerical computations has been reported within the same range as the present study. Specifically, from dissolution studies of carbon rods in liquid steel,[16] agreement between numerical and experimental results within a factor of 2 was achieved using turbulent flow correlations (for mass transfer) while there was one order of magnitude difference when laminar flow correlations were used.

VII. CONCLUSIONS

It has been demonstrated that the proposed probe can be used for measurement of flow velocities in unknown flow fields upon proper calibration. It is essential that for flow measurements in the broader vicinity of solid boundaries or free surfaces, detailed calibration experimentation be carried out in order to quantify the effect of the system geometry on the calibration results.

The results from part B of the study demonstrate that for the range of velocities 0 to 40 cm/s, the relationship between sphere melting time and flow velocity is linear. Bath superheat in the range of 40 °C to 100 °C generally shifts the calibration curves in parallel, with higher superheats requiring lower melting times. At higher bath superheats, it is expected that the slope will be higher. This trend has been observed in the case of small sphere diameters at 100 °C superheat.

The results from part C showed the effect of system geometry on the sphere melting time. The calibration results obtained in part B of the study were used to measure flow velocities in an induction furnace. From the modeling results presented in part D of the study, it was shown that numerical and experimental results are in good agreement for all three sizes of spheres that were used in the flow measurements.

APPENDIX

As discussed in a number of publications,[2,16,30,31,52–57] the fluid flow field in an induction furnace may be described by the equation of continuity and the equations of motion, which in cylindrical coordinates are as follows:

equation of continuity

$$\frac{1}{r}\frac{\partial}{\partial r}(\rho r V_r) + \frac{\partial}{\partial z}(\rho V_z) = 0 \qquad [A1]$$

momentum balance in the z direction

$$\frac{1}{r}\left[\frac{\partial}{\partial r}(\rho r V_r V_z)\right] + \frac{\partial}{\partial z}(\rho V_z^2) = -\frac{\partial p}{\partial z} + \frac{1}{r}\frac{\partial}{\partial r}\left(\mu_{\text{eff}} r \frac{\partial V_z}{\partial r}\right) + 2\frac{\partial}{\partial z}\left(\mu_{\text{eff}}\frac{\partial V_z}{\partial z}\right) + \frac{1}{r}\frac{\partial}{\partial r}\left(\mu_{\text{eff}} r \frac{\partial V_r}{\partial z}\right) + \bar{F}_z \qquad [A2]$$

momentum balance in the r direction

$$\frac{1}{r}\left[\frac{\partial}{\partial r}(\rho r V_r^2)\right] + \frac{\partial}{\partial z}(\rho V_r V_z) = -\frac{\partial p}{\partial r} + \frac{2}{r}\frac{\partial}{\partial r}\left(\mu_{\text{eff}} r \frac{\partial V_r}{\partial r}\right) + \frac{\partial}{\partial z}\left(\mu_{\text{eff}}\frac{\partial V_r}{\partial z}\right) + \frac{\partial}{\partial z}\left(\mu_{\text{eff}}\frac{\partial V_z}{\partial r}\right) - \frac{2V_r\mu_{\text{eff}}}{r^2} + \bar{F}_r \qquad [A3]$$

where V_r and V_z are the radial and vertical components

of the velocity, respectively, p is pressure, ρ the fluid density, $\bar{F}_r$ and $\bar{F}_z$ are the average electromagnetic force components in the radial and vertical directions, respectively, and μ_{eff} is the effective viscosity which is calculated using the $\kappa - \varepsilon$ model of turbulence which is presented subsequently.

The effective viscosity μ_{eff} is defined as

$$\mu_{\text{eff}} = \mu_t + \mu \qquad [A4]$$

where μ_t is the turbulent viscosity and μ the laminar viscosity. The turbulent viscosity is defined as

$$\mu_t = \frac{C_\mu \rho k^2}{\varepsilon} \qquad [A5]$$

where κ and ε are the turbulent kinetic energy and the turbulent kinetic energy dissipation rate, respectively, while C_μ is a constant.

The spatial distribution of the quantities κ and ε can be obtained through the solution of the conservation equations for these variables which take the following form in the cylindrical coordinate system:

conservation equation for turbulent kinetic energy

$$\frac{\partial}{\partial z}(\rho V_z k) + \frac{1}{r}\frac{\partial}{\partial r}(\rho r V_r k) - \frac{\partial}{\partial z}\left(\frac{\mu_{\text{eff}}}{\sigma_k}\frac{\partial k}{\partial z}\right) - \frac{1}{r}\frac{\partial}{\partial r}\left(r\frac{\mu_{\text{eff}}}{\sigma_k}\frac{\partial k}{\partial r}\right) = G - D \qquad [A6]$$

where

$$G = \mu_t\left\{2\left[\left(\frac{\partial V_z}{\partial z}\right)^2 + \left(\frac{\partial V_r}{\partial r}\right)^2 + \left(\frac{V_r}{r}\right)^2\right] + \left(\frac{\partial V_z}{\partial r} + \frac{\partial V_r}{\partial z}\right)^2\right\} \qquad [A7]$$

$$D = \rho\varepsilon \qquad [A8]$$

σ_k being a constant.

conservation equation for turbulent kinetic energy dissipation rate

$$\frac{\partial}{\partial z}(\rho V_z \varepsilon) + \frac{1}{r}\frac{\partial}{\partial r}(\rho r V_r \varepsilon) - \frac{\partial}{\partial z}\left(\frac{\mu_{\text{eff}}}{\sigma_\varepsilon}\frac{\partial \varepsilon}{\partial z}\right) - \frac{1}{r}\frac{\partial}{\partial r}\left(r\frac{\mu_{\text{eff}}}{\sigma_\varepsilon}\frac{\partial \varepsilon}{\partial r}\right) = G\frac{C_1\varepsilon}{k} - \frac{C_2\rho\varepsilon^2}{k} \qquad [A9]$$

where C_1, C_2, and σ_ε are constants.

It follows that ultimately the solution of the fluid flow problem requires the simultaneous solution of five differential Eqs. ([A1] through [A3], [A6], and [A9]). In addition, the numerical solutions obtained will depend upon the values chosen for the constants that are involved in the conservation equations for κ and ε. The values that are adopted for these constants are[50]

$$C_\mu = 0.09 \quad C_1 = 1.44 \quad C_2 = 1.92$$
$$\sigma_k = 1.0 \quad \sigma_\varepsilon = 1.3$$

The form of the turbulence model that has been presented previously is valid only for fully turbulent flows. Close to solid wall and some other interfaces there are inevitably regions where the local Reynolds number of turbulence ($R_t = \kappa^2/(\nu\varepsilon)$, where ν is the kinematic viscosity) is so small that viscous effects predominate over turbulent ones. The wall function method which is analytically described in a study by Launder and Spalding[50] was adopted, while the value that was introduced for the wall roughness variable is that for a smooth wall.

In this study, the results of the flow numerical model were clearly demonstrating that the flow is not fully turbulent in all regions of the induction furnace. As a result, it was decided that the model should be modified accordingly. Several authors have sought to devise turbulence model equations which are valid throughout the laminar, semilaminar, and fully turbulent regions. For the case of one-equation turbulence models, the studies by Glusko[58] and Wolfshtein[59] are some examples. The modifications to the original $\kappa - \varepsilon$ turbulence model (as was described earlier) that were adopted in the present study are according to the recommendations of Jones and Launder[60,61] who extended the $\kappa - \varepsilon$ model to low Reynolds number flows. These recommendations are also summarized in the article of Launder and Spalding.[50] In this version of the model, κ and ε are determined from the following pair of equations written in a general condensed form:

$$\frac{D\varepsilon}{Dt} = \frac{1}{\rho}\frac{\partial}{\partial x_j}\left[\left(\frac{\mu_t}{\sigma_\epsilon} + \mu\right)\frac{\partial \varepsilon}{\partial x_j}\right] + C_1\frac{\varepsilon}{k}\frac{\mu_t}{\rho}\frac{\partial V_i}{\partial x_j}\left(\frac{\partial V_i}{\partial x_j} + \frac{\partial V_j}{\partial x_i}\right) - \frac{C_2\varepsilon^2}{k} - 2.0\frac{\nu\mu_t}{\rho}\left(\frac{\partial^2 V_i}{\partial x_j \partial x_i}\right)^2 \qquad [A10]$$

$$\frac{Dk}{Dt} = \frac{1}{\rho}\frac{\partial}{\partial x_j}\left[\left(\frac{\mu_t}{\sigma_k} + \mu\right)\frac{\partial k}{\partial x_j}\right] + \frac{\mu_t}{\rho}\frac{\partial V_i}{\partial x_j}\left(\frac{\partial V_i}{\partial x_j} + \frac{\partial V_j}{\partial x_i}\right) - 2\nu\left(\frac{\partial k^{1/2}}{\partial x_j}\right)^2 - \varepsilon \qquad [A11]$$

In the above equations, C_1, σ_k, and σ_ϵ retain the values assigned to them for high Reynolds numbers while C_μ and C_2 are held to vary with the turbulence Reynolds number according to the following formulas:

$$C_\mu = 0.09 \exp\left[-2.5/(1 + R_t/50)\right] \qquad [A12]$$

$$C_2 = 1.92\left[1.0 - 0.3 \exp - R_t^2\right] \qquad [A13]$$

According to Launder and Spalding,[50] with the modifications done to the original Eqs. [A6] and [A9], the viscosity now exerts influence on the levels of κ and ε in two additional ways: first, laminar diffusive transport becomes of increasing importance as the wall is approached, and second, extra distraction terms have been included which are of some significance in the viscous and transitional regions.

Boundary conditions

In principle, the boundary conditions which are required to complete the statement of the problem specify zero velocity at the solid surfaces, zero shear at the free surface, and the existence of symmetry about the centerline. Furthermore, the quantities κ and ε are set equal

to zero at the solid surfaces and their gradients are stipulated to be zero at the free surfaces. With reference to the detailed schematic cross section of the induction furnace in Figure 11, the boundary conditions for the flow model can be written as follows (point A in Figure 11 represents point (0,0) for the (r, z) coordinate system):

centerline ($\forall \mathbf{z}$ at $\mathbf{r} = 0$) or AD boundary

$$\frac{\partial k}{\partial r} = \frac{\partial \varepsilon}{\partial r} = \frac{\partial V_r}{\partial r} = \frac{\partial V_z}{\partial r} = 0 \qquad [A14]$$

top of melt ($\forall r$ at $z = 0$) or AB boundary

$$\tau_{zr} = \tau_{rz} = 0 \quad \text{and} \quad \frac{\partial k}{\partial z} = \frac{\partial \varepsilon}{\partial z} = 0 \qquad [A15]$$

side wall of crucible ($\forall z$ at $r = R$, where R is the internal radius of crucible) or BC boundary

$$V_r = V_z = k = \varepsilon = 0 \qquad [A16]$$

bottom wall of crucible ($\forall r$ at $z = L$, where L is the melt height) or CD boundary

$$V_r = V_z = k = \varepsilon = 0 \qquad [A17]$$

As we discussed earlier, for the near wall region using the formulation for the fully turbulent model, the wall function method was used, while the low Reynolds number turbulence model was adopted which takes care of the transitional regimes. Both of these formulations were originally developed based on the universal velocity distribution for turbulent boundary layers without pressure gradient and body forces, the adoption of which in the present model might contribute to the margin of error.

LIST OF SYMBOLS

$\bar{F}_z$	average electromagnetic force component in the vertical direction
Re	Reynolds number
Tu	Turbulent intensity
Sh	Sherwood number
Sc	Schmidt number
V_r	radial component of the velocity
V_z	vertical component of the velocity
p	pressure
ρ	fluid density
$\bar{F}_r$	average electromagnetic force component in the radial direction
$\bar{F}_z$	average electromagnetic force component in the vertical direction
μ_t	turbulent viscosity
κ	turbulent kinetic energy
ε	rate of dissipation of turbulent kinetic energy

REFERENCES

1. Erach D. Tarapore and J.W. Evans: *Metall. Trans. B*, 1976, vol. 7B, pp. 343-351.
2. Erach D. Tarapore, James W. Evans, and John Langfeldt: *Metall. Trans. B*, 1977, vol. 8B, pp. 179-84.
3. J. Szekely, C.W. Chang, and W.E. Johnson: *Metall. Trans. B*, 1977, vol. 8B, pp. 514-17.
4. M. Saiben: *Rev. Sci. Instrum.*, 1965, vol. 36, pp. 945-49.
5. J.C. Hill and C.A. Sleicher: *Rev. Scient. Instrum.*, 1971, vol. 42, pp. 1461-68.
6. D.G. Malcolm: *J. Fluid Mech.*, 1969, vol. 37, pp. 701-14.
7. M. Hoff: *Instrum. Cont. Syst.*, 1969, vol. 42, pp. 83-86.
8. I.A. Platienks: *Magnit. Gidrod.*, 1971, vol. 7, pp. 140-42.
9. P.S. Lykoudis and F.P. Dunn: *Int. J. Heat Mass Transfer*, 1973, vol. 16, pp. 1439-52.
10. R.J. Holroyd: *DISA Inform.*, 1980, vol. 25, pp. 19-24.
11. C.A. Sleicher and G.B. Lim: in *Proceedings of the Symposium on Turbulence in Liquids*, University of Missouri–Rolla, Rolla, 1975, pp. 563-70.
12. P. Cremer and A. Alemany: *J. Méc. Appl.*, 1981, vol. 5 (1), pp. 37-50.
13. E. Taberlet and Y. Fautrelle: *J. Fluid Mech.*, 1985, vol. 159, pp. 409-31.
14. A. Murthy and J. Szekely: *Metall. Trans. B*, 1983, vol. 14B, pp. 499-502.
15. J. Szekely, C.W. Chang, and R.E. Ryan: *Metall. Trans. B*, 1977, vol. 8B, pp. 333-38.
16. N. El-Kaddah, J. Szekely, and G. Carlsson: *Metall. Trans. B*, 1984, vol. 14B, pp. 633-40.
17. T.C. Hsiao: MEFOS Report No. 79063E.
18. D.J. Moore and J.C.R. Hunt: *Prog. Astronautics Aeronautics*, 1983, vol. 84, pp. 359-73. (This is the revised version of the original paper in the *Proc. 3rd Beer-Sheva Int. Seminar on MHD Flows and Turbulence*, H. Branover, P.S. Lykoudis, and A. Yakhot, eds., Beersheva, Israel, Mar. 23–27, 1981).
19. D.J. Moore: Ph.D. Dissertation, Cambridge University, Cambridge, United Kingdom, 1982.
20. D.C. Lillicrap and D.J. Moore: *Proc. Electroheat and metals Conf.*, University of Cambridge, Cambridge, United Kingdom, Sept. 21–23, 1982.
21. D.C. Lillicrap: in *Proc. Symp. of the International Union of Theoretical and Applied Mechanics*, H.K. Moffatt and M.R.E. Proctor, eds., 1982, pp. 46-56.
22. A. Moros, J.C.R. Hunt, and D.C. Lillicrap: *Progress in Astronautics and Aeronautics*, 1985, vol. 100, pp. 706-15; 4th Beersheva Int. Seminar on MHD Flows and Turbulence, Beersheva, Israel, 1984.
23. H. Schlichting: *Boundary Layer Theory*, 7th ed., McGraw Hill Book Company, Maidenhead, England, 1979.
24. Kai Grjotheim, Conrad Krohn, Roger Naeumann, and Knut Torklep: *Metall. Trans.*, 1970, vol. 1, pp. 3133-41.
25. Kai Grjotheim, Conrad Krohn, Roger Naeumann, and Knut Torklep: *Metall. Trans.*, 1971, vol. 2, pp. 199-204.
26. B. Berge, K. Grjotheim, C. Krohn, R. Naeumann, and K. Torklep: *Metall. Trans.*, 1973, vol. 4, pp. 1945-52.
27. J. Szekely: *J. Iron Steel Inst.*, 1964, vol. 202, pp. 505-08.
28. K. Nakanishi, J. Szekely, T. Fujii, Y. Mihara, and S. Iwaoka: *Metall. Trans. B*, 1975, vol. 6B, pp. 111-18.
29. J. Szekely and K. Nakanishi: *Metall. Trans. B*, 1975, vol. 6B, pp. 245-56.
30. J. Szekely and C.W. Chang: *Ironmaking and Steelmaking*, 1977, vol. 3, pp. 196-204.
31. J. Szekely and C.W. Chang: *Ironmaking and Steelmaking*, 1977, vol. 3, pp. 190-95.
32. A.T. Hjelmfelt and L.F. Mockros: *Appl. Sci. Res.*, 1966, vol. 16 (2), pp. 149-61.
33. C. Vivès, R. Ricou, and A. Chambarel: French Patent ANVAR No. 79/19818, 1979.
34. R. Ricou and C. Vivès: *Int. J. Heat Mass Transfer*, 1982, vol. 25, pp. 1579-88.
35. C. Vivès and R. Ricou: *Metall. Trans. B*, 1985, vol. 16B, pp. 377-84.
36. C. Vivès and R. Ricou: *Metall. Trans. B*, 1985, vol. 16B, pp. 227-35.
37. J.L. Meyer, N. El-Kaddah, J. Szekely, C. Vivès, and R. Ricou: *Metall. Trans. B*, 1987, vol. 18B, pp. 529-38.
38. J.L. Meyer, F. Durand, R. Ricou, and C. Vivès: *Metall. Trans. B*, 1984, vol. 15B, pp. 471-78.
39. A.C. Mikrovas: Ph.D. Thesis, University of Toronto, Toronto, 1992.
40. Ben Q. Li: Alcoa Technical Center, USA, private communication, 1992.
41. A.R. Johnson: *Light Met.*, 1978, vol. 1, pp. 45-58.
42. A.T. Tabereaux and R.B. Hester: *Light Met.*, 1984, vol. 1, pp. 519-39.

43. B.E. Bradley, E.W. Dewing, and J.N. Rogers: *Light Met.*, 1984, vol. 1, pp. 541-52.
44. A. Pant, A. Langille, R. Roy, and M. Wells: *Light Met.*, 1986, vol. 2, pp. 541-50.
45. V.T. Morgan: *Advances in Heat Transfer*, Academic Press, 1975, vol. 11, pp. 199-264.
46. J. Szekely, H.H. Grevet, and N. El-Kaddah: *Int. J. Heat Mass Transfer*, 1984, vol. 27, pp. 1116-21.
47. J.H. Grevet, J. Szekely, and N.L. Kaddah: *Int. J. Heat Mass Transfer*, 1982, vol. 25, pp. 487-92.
48. V.G. Zhilin, K.V. Zvyagin, Y.P. Ivochkin, and A.A. Oksman: *Diagnostics of Liquid Metal Flows Using Fibre-Optic Velocity Sensor*, J. Lielpeteris and R. Moreau, eds., Kluwer Academic Publishers, Lancaster, United Kingdom, 1989, pp. 373-79.
49. G. Bendzsak: Hatch Associates Ltd., Toronto, Canada, private communication, 1990.
50. B.E. Launder and D.B. Spalding: in *Computer Methods in Applied Mechanics and Engineering*, J.H. Argyris, W. Prager, and A.M.O. Smith, eds., 1974, vol. 3 (1), pp. 269-89.
51. S.V. Patankar: *Numerical Heat Transfer and Fluid Flow*, Hemisphere Publishing Corporation, New York, NY, 1980.
52. J.W. Evans and S.D. Lympany: *Metall. Trans. B*, 1983, vol. 14B, pp. 306-08.
53. N. El-Kaddah and J. Szekely: *J. Fluid Mech.*, vol. 133, pp. 37-46.
54. J.N. Barbier, Y.R. Fautrelle, J.W. Evans, and P. Cremer: *J. Mec. Théor. Appl.*, 1982, vol. 1 (3), pp. 533-56.
55. N. El-Kaddah and J. Szekely: *Metall. Trans. B*, 1983, vol. 14B, pp. 401-10.
56. N. El-Kaddah and J. Szekely: *Metall. Trans. B*, 1984, vol. 15B, pp. 183-86.
57. J.L. Meyer, F. Durand, R. Ricou, and C. Vivès: *Metall. Trans. B*, 1984, vol. 15B, pp. 471-78.
58. G.S. Glasko: *Izv. Acad. Nauk SSSR Mekh.*, 1965, No. 4, pp. 13-20.
59. M.W. Wolfshtein: *Int. J. Heat Mass Transfer*, 1969, vol. 12, pp. 301-18.
60. W.P. Jones and B.E. Launder: *Int. J. Heat Mass Transfer*, 1973, vol. 16, pp. 1119-130.
61. W.P. Jones and B.E. Launder: *Int. J. Heat Mass Transfer*, 1972, vol. 15, pp. 301-14.